coatings

MDPI

Article

Robust Superhydrophobic and Repellent Coatings Based on Micro/Nano SiO_2 and Fluorinated Epoxy

Xiaoye Huang and Ruobing Yu *

School of Materials Science and Engineering, East China University of Science and Technology, No. 130 Meilong Road, Lingyun District, Shanghai 200237, China; y30180417@mail.ecust.edu.cn
* Correspondence: rbyu@ecust.edu.cn; Tel.: +86-133-3198-2086

Abstract: Superhydrophobic surfaces possess low mechanical strength, and can be easily contaminated by fluids with low surface tension, such as oil; this hinders their practical applications. In this study, fluorinated epoxy was prepared through the thiol-ene click reaction at first. The superhydrophobic surface with high oil-repellency was prepared by the addition of unmodified nano-SiO_2 and micron-SiO_2 to the fluorinated epoxy. The effect of the ratio of micro- and nano-silica particles on the morphology and wettability of the coating was investigated. It was shown that a re-entrant structure appears and FEP-S coating has good liquid repellency when the amounts of nano-SiO_2 and micro-SiO_2 are equal. The contact angles of the FEP-S coating (coating with the best liquid repellent performance) for water, glycerol, ethylene glycol, and diiodomethane were 158.6° ± 1.1°, 152.4° ± 0.9°, 153.4° ± 1.3°, and 140.7° ± 0.9°, respectively. In addition, the superhydrophobic coatings possess excellent mechanical and chemical durability, excellent performance in self-cleaning, corrosion resistance, and anti-icing properties. The preparation method of superhydrophobic coating is relatively simple; therefore, it has a wide range of applications and can also be applied to various substrates.

Keywords: superhydrophobic; oleophobic; click chemistry; silica; fluorinated epoxy

Citation: Huang, X.; Yu, R. Robust Superhydrophobic and Repellent Coatings Based on Micro/Nano SiO_2 and Fluorinated Epoxy. *Coatings* **2021**, *11*, 663. https://doi.org/10.3390/coatings11060663

Academic Editors: N. P. Prorokova and Ioannis Karapanagiotis

Received: 10 April 2021
Accepted: 28 May 2021
Published: 31 May 2021

1. Introduction

The superhydrophobic surface is a surface where the water contact angle is greater than 150° and the contact angle hysteresis is lower than 10°. Superhydrophobic surfaces have wide applications in self-cleaning [1], antifouling [2], anti-icing [3,4], anti-corrosion [5,6], oil transfer, and oil-water separation [7,8]. Extensive literature is available related to the preparation of superhydrophobic surfaces. However, in practical applications, the superhydrophobic surfaces inevitably encounter some problems. After contact with organic liquids with low surface tension, and even fingerprints, the surface will lose their superhydrophobicity. Therefore, superhydrophobic surfaces which can repel both water and oil have more practical applications as compared with ordinary superhydrophobic surfaces.

However, superoleophobic surfaces have low surface energy and their manufacturing is difficult than that of ordinary superhydrophobic surfaces. In addition, superoleophobic surfaces possess more delicate structures, such as re-entrant structures. The superoleophobic surfaces can repel fluids with low surface tension when the droplet is in the Cassie-Baxter state. Since Tuteja et al. [9] developed a superoleophobic surface by introducing re-entrant features in 2007, several researchers have investigated the superoleophobic surfaces by designing a hierarchical structure similar to a re-entrant structure (e.g., hanging structure [10,11], inverted trapezoid structure [12,13], mushroom shape [8,14], flower shape [15–17], bowstring shape [18], nano-filament [19,20] and candle soot [21]). However, re-entrant structures are more delicate than simple hierarchical structures, which are difficult to manufacture and require complex techniques and expensive equipment, for example, electrospinning [22,23], lithography [24,25], templating [21,26], laser ablation [27–29], anodic oxidation [30,31], vapor deposition [2,32], plasma etching [33–35], and other combina-

tional approaches. Owing to the structural requirements and limitations of the professional equipment of the superoleophobic coating, it is more practical to fabricate a superhydrophobic and oleophobic coating by a simple method. In fact, the spray-coating or drop-coating method, which is based on an adhesive (e.g., Epoxy [36,37], polyurethane [38], inorganic adhesive [39] and 3M glue [14]) and nanoparticles (e.g., SiO_2 [40], TiO_2 [14] and ZnO [17]), is simple and economical for the fabrication of superhydrophobic and oleophobic coatings.

Xiong et al. [40] synthesized two block copolymers by anionic polymerization, poly [3-(triisopropyloxysilyl)propyl methacrylate]-block-poly(perfluorooctylethyl methacrylate) (PIPSMA-b-PFOEMA) and poly(tert-butyl acrylate) (PIPSMA-b-PtBA), which were grafted onto SiO_2 through the Stober method in the presence of HCl. The as-prepared bi-functional silica solution was drop-casted onto epoxy glue (first coated on a glass slide). The coating can repel water and oil with good adhesive strength. However, the synthesis of two block copolymers and bi-functional silica particles is complex.

Wang et al. [36] added nano-silica and carbon nanotubes to epoxy resin (EP)/modified poly (vinylidene fluoride) (MPVDF)/fluorinated ethylene propylene (FEP) composite, and obtained a superamphiphobic coating with a high wear life and corrosion resistance.

Su et al. [41] first obtained modified micron- and nano-silica by grafting epoxy resin, and then sprayed these on the glass slides in turn with a spray gun. The coating was superhydrophobic. The preparation and curing time of the coating were long.

Li et al. [37] prepared fluorinated nano-SiO_2 particles by the sol-gel method and used these as a sheath with a core of epoxy solution to prepare a superamphiphobic coating by a coaxial electrospray method. However, the wear resistance of the coating was low.

Zhang et al. [42] applied bisphenol A diglycidyl ether (BADGE) epoxy resin and unmodified multi-walled carbon nanotubes (MWCNTs) to establish a superhydrophobic coating, which exhibited good mechanical durability and anti-icing performance.

Xiu et al. [43] mixed silica particles (100 nm) and bisphenol A diglycidyl ether, hexahydro-4-methylphthalic anhydride, and imidazole in toluene and coated the dispersion on a glass slide, which was then cured for 4 h at 150 °C. The epoxy was etched away and silica nanoparticles were exposed on the surface by plasma etching. The coating was then dipped in perfluorinated octyl trichlorosilane (PFOS) to form a superhydrophobic surface.

Han et al. [44] prepared raspberry-like hollow SnO_2 nanoparticles by a hydrothermal method and modified it with 1H, 1H, 2H, 2H-Perfluorodecyltriethoxysilane (FAS17). The modified SnO_2 and SiO_2 were added to the epoxy to obtain a robust superamphiphobic coating with good stability.

Peng et al. [45] first sprayed epoxy resin on the matrix as an adhesive, and then zinc oxide and silica particle solution were coated on the surface to construct a rough surface. The surface was wear-resistant and superamphiphobic.

Aslanidou et al. [46] have prepared a water soluble siloxane emulsion enriched with silica nanoparticles (7 nm) and sprayed it on the surface of marble and sandstone. The coating is superhydrophobicity and superoleophobicity. It was shown that when the nanoparticle concentration is 2% w/w, the coating has best superhydrophobicity and superoleophobicity.

From the aforementioned discussion, there are two procedures to prepare the coating by "glue + particles". One is to spray the mixture of particles and glue, which can improve the adhesive strength of the coating; however, it is difficult to achieve oleophobic properties because the particles are covered with the glue. The other method is to coat the particle solution on the surface of the glue. The exposed particles can easily fall owing to the low adhesive strength. In this study, we aimed to prepare a superhydrophobic and oleophobic coating using a mixture of particles and glue. To achieve oleophobic performance, a novel fluorinated epoxy, which can provide both good adhesion and strong liquid repellency, was employed as the glue. The synthesis of fluorinated epoxy containing epoxy groups and long perfluoroalkyl chains was based on the modified Zhang's method [1,47,48]. This novel fluorinated epoxy was prepared by introducing 1H, 1H, 2H, 2H-perfluorodecyl acrylate (PFDA), and glycidyl methacrylate (GMA) into

pentaerythritol tetra (3-mercaptopropionate) (PETMP) via a simple and fast thiol-ene click reaction. By adding micro- and nano-silica particles to fluorinated epoxy and adjusting their proportions, we obtained a superhydrophobic and oleophobic coating with different micro/nanostructures and different liquid repellent properties.

2. Materials and Methods

2.1. Materials

Acetone (99.5%) was purchased from General-Reagent; PFDA was obtained from Adamas-beta. GMA and PETMP were supplied by Aladdin; 2-methylimidazole (GC), 2, 2-bimethoxy-2-phenylacetophenone (DMPA), micron silicon dioxide (W-180, with an average particle size of 2 μm), and nano silicon dioxide (S861577, with an average particle size of 20 nm) were sourced from Macklin.

2.2. Preparation of Fluorinated Epoxy

Fluorinated epoxy was fabricated by a modified method of Zhang et al. [1,47,48]. We applied thiol-ene click chemistry reaction (Figure 1) to prepare fluorinated epoxy as follows: 0.3 mol GMA, 0.1 mol PETMP and 0.1 mol PFDA were mixed in acetone, and then the mixture was treated by ultrasonic for 10 min before adding 0.001 mol DMPA. The solution was exposed to ultraviolet radiation (365 nm, 300 W) for 1 h at 25 °C.

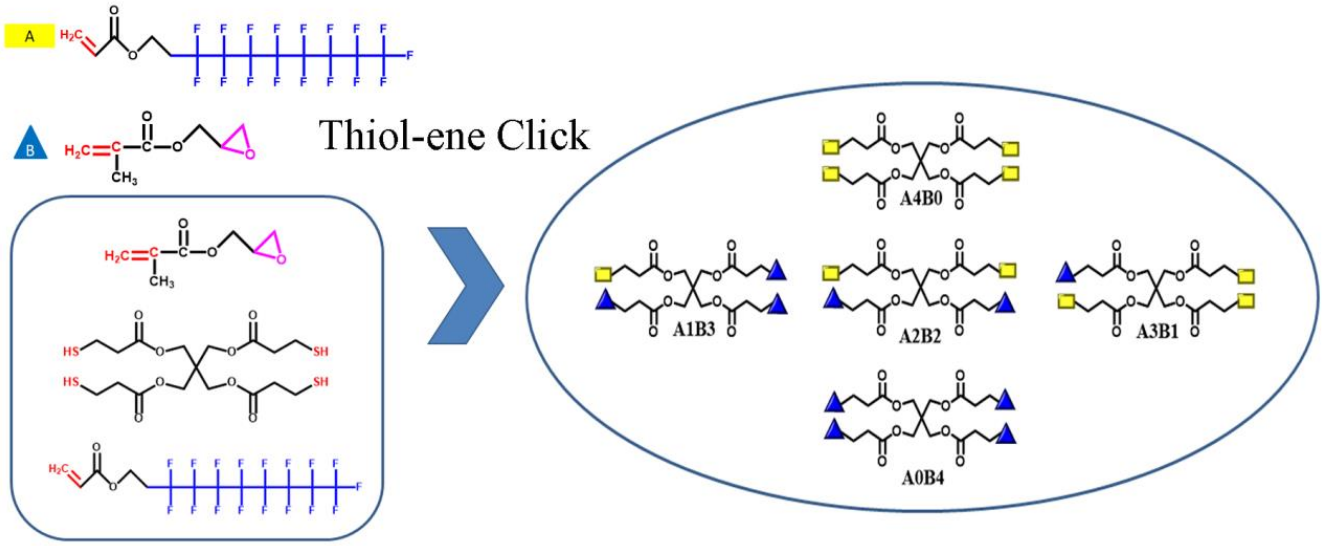

Figure 1. Scheme for preparation of fluorinated epoxy via thiol-ene click method.

2.3. Preparation of Micro/Nano-Silica Coatings by Spray-Coating Approach

The procedure for the preparation of the coating is shown in Figure 2. First, nano- and micron-SiO_2 particles with mass ratios of 0:1, 1:0, 2:1, 1:2, and 1:1 were ultrasonically dispersed in 3 g of fluorinated epoxy (50 wt% in acetone solution) for 20 min. Subsequently, five as-prepared solutions were added to 15 mg GC and magnetically ultrasonicated for 20 min at 25 °C. Solutions with five different ratios were obtained (0:1, 1:0, 2:1, 1:2, and 1:1) and marked as S1, S2, S3, S4, and S5, respectively.

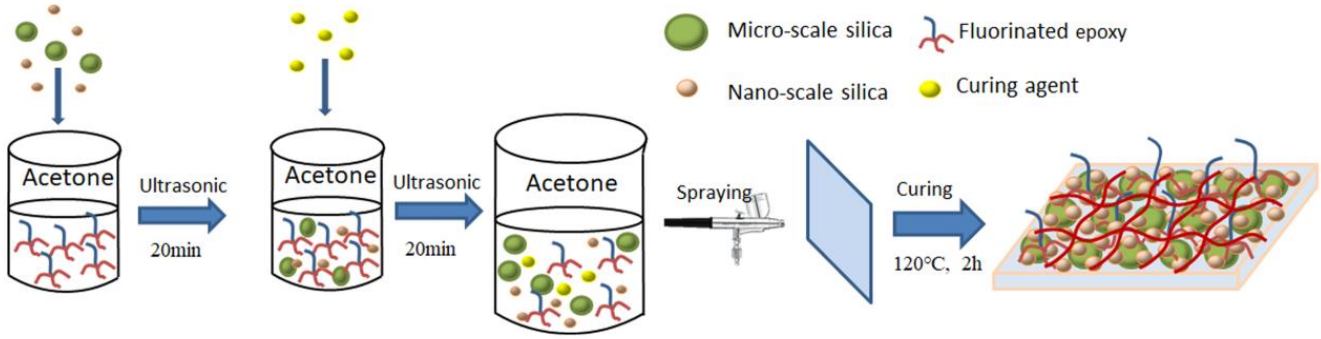

Figure 2. Scheme for preparation of coating by spraying.

Before spray coating, all glasses and aluminum foil were placed in deionized water and ethanol for ultrasonic cleaning and then blow-dried in air. Subsequently, the as-prepared solution was sprayed onto the slides or aluminum foil by a spray gun with a nozzle diameter of 0.5 mm and 0.3 MPa compressed air (Youlun S-131, Master airbrush). The operating air was controlled by an airbrush compressor (Lotus T-300K), and the distance between the airbrush and the substrate was set at approximately 15 cm. The coated slides were placed on a heating platform at 80 °C for 5 min to remove the solute and then placed in an oven at 120 °C for 2 h.

We named the coating with the best liquid repellent performance as FEP-S (with solution S5). In order to understand the comprehensive property of FEP-S, the surface chemical composition, mechanical and chemical stability and self-cleaning properties and anti-icing performance were also evaluated.

2.4. Analysis and Testing Methods

- Abrasion test

Sandpaper (600 grid) and a standard weight (100 g) were used to abrade FEP-S coating at a pressure of 1 kPa. The sandpaper was placed on a horizontal surface and the coating was placed on the sandpaper. A weight was placed on the back of the coating, and the coating was slid along the ruler at 1 cm/s on the sandpaper surface, 10 cm to the right, and 10 cm to the left for a cycle test. We measured the CA of FEP-S coating for the four liquids after every 10 cycles.

- Cross cut adhesion test

With a cross-hatch cutter (BEVS2202, 2 mm), as per the Chinese National Standard (GB/T 9286-1998), a lattice pattern was cut with equidistant spacing on the coating surface, and commercial cellophane tape was applied over the lattice for 5 min and then peeled off.

The adhesion level of the coating, as obtained from GB/T 9286-1998, is presented in Table 1.

- Chemical stability test

Water droplets with different pH values ranging from 1 to 14 were placed on the surface of the superhydrophobic coating to test the chemical stability.

The chemical stability of the FEP-S coating was further tested by immersing the samples in a strong acid (HCl, pH = 1) or basic solution (NaOH, pH = 14) at 25 °C for 1 h. The sample was then rinsed with distilled water for 3 min, and oven-dried at 80 °C for 10 min. Subsequently, the WCAs of the samples were recorded.

Table 1. Adhesion level of cross-cut method.

Adhesion Level	Description	Percent (%) Area Removed
0	The edges of the square are completely smooth, none of the squares of the lattice are detached	0%
1	Small flakes of the coating are detached at intersections, and less than 5% of the area is affected	<5%
2	Small flakes of the coating are detached along edges and at the intersections of cuts	5–15%
3	The coating has flaked along the edges and on parts of the squares	15–35%
4	The coating has flaked along the edges of the cuts in large ribbons and whole squares have detached	35–65%
5	Severe flaking and detachment across entire square	>65%

- Self-cleaning test

A self-cleaning test was conducted using carbon black powder and $CuSO_4$ powder as contaminants on the surface of the FEP-S coating. Water droplets were dripped onto the coated glass through a disposable dropper.

The repellent properties of the FEP-S coating were tested by immersing the samples in common liquids that are used in daily life (e.g., water, coffee, cola, juice, tea, and soybean milk) for 5 min, and then taken out to observe the surface.

- Anti-icing test

The ice delay property of the FEP-S coating was tested by dropping water (~0.05 mL) on the original glass slide and the coated glass slide, and these slides were placed in a freezer at −18 °C. The slides were taken out after every 30 s to observe the state of the water droplets.

Dynamic anti-icing of the coating was also performed in the freezer at −18 °C. Bare glass and coated glass slides were placed in the freezer for 24 h, and a few drops of water at 0 °C were dropped on the coating to observe the state of droplets falling on the coating.

- Other characterization

The FEP-S coating used in the SEM, EDS and XPS tests is based on an aluminum foil substrate, and the other characterizations are based on a glass slide substrate. The morphology (SEM photograph) and the element distribution of the coating was studied by field emission scanning electron microscopy (FE-SEM, S-4800, Hitachi, Japan) equipped with energy dispersive spectroscopy (EDS mapping). The sample was attached to a conductive adhesive and sprayed with gold. The acceleration voltage of the instrument was 10–20 kV.

The content and distribution of the surface elements of FEP-S were characterized by X-ray photoelectron spectroscopy (XPS, Thermo Scientific Escalab 250Xi, Massachusetts, MA, USA). Before XPS test, FEP-S coating was placed in a vacuum oven at 80 °C for 12 h. The contact angles (CAs) of the different liquids on the coating were measured using the contact angle tester (JC 2000D2, Zhongchen, China) at 25 °C. All CA values were determined by averaging the values at five different points on each sample surface.

The sliding angles (SAs) were measured with a contact angle system (Kruss DSA 100S, Hamburg, Germany).

IR data of fluorinated epoxy and a mixture of PFDA, GMA and PETMP were obtained by Fourier transform infrared spectrometer (Nicolet 6700, Thermo Fisher, Waltham, MA, USA) operating over the frequency range of 4000–500 cm^{-1}. The samples were prepared via potassium bromide tableting.

Proton nuclear magnetic resonance (1H-NMR) spectra were obtained using a III-400 NMR spectrometer (Bruker Avance, Zurich, Switzerland), and deuterated chloroform was used as the solvent. TMS was used as the internal standard.

3. Results and Discussion

3.1. Preparation and Characterization of Fluorinated Epoxy

Fluorinated epoxy was manufactured by a thiol-ene click reaction as proposed by Zhang [1,47,48]. The radical reaction is rapid and has no byproducts.

The chemical structure of the fluorinated epoxy was characterized by Fourier transform infrared spectroscopy (FT-IR) and proton nuclear magnetic resonance (1H-NMR). The comparison of typical IR spectra of the reactants (mixture of PETMP, GMA, and PFDA) and products (fluorinated epoxy) are presented in Figure 3. Absorption peaks of epoxy groups could be observed in both reactants and products, with wavelengths of 937 cm^{-1} and 906 cm^{-1}, respectively. The epoxy absorption peak was introduced into fluorinated epoxy by GMA, which can be cured and cross-linked under the action of a curing agent (GC) to achieve high bonding strength with the substrate. The absorption peaks at wavelengths of 1730 cm^{-1} for the reactants and products were the stretching vibration peaks of C=O, the absorption peak was due to the ester group present in the three reactants, and did not disappear after the clicking reaction. The absorption peaks of -CF_2 also presented in reactant and product, at wavelengths of 1148 cm^{-1} and 1204 cm^{-1} respectively. Compared with the reactants, the peak of C=C at 1636 cm^{-1} and the peak of -SH at 2585 cm^{-1} disappeared in the product owing to completion of reaction of -SH with C=C to form a -CS bond, which also led to an increase in the -CH peak around 2918 cm^{-1} in the product.

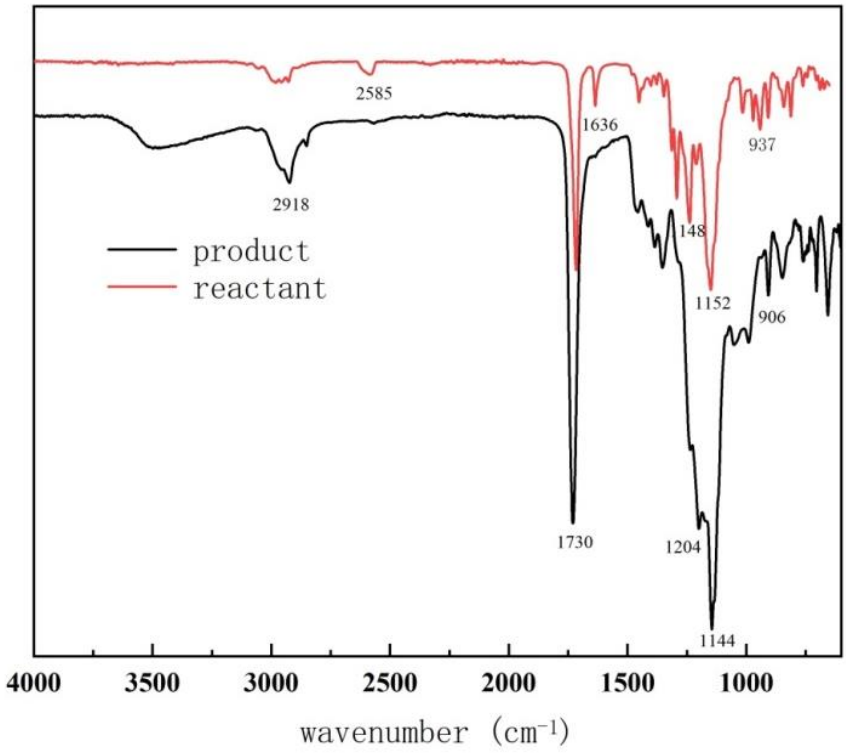

Figure 3. FT-IR spectra of the reactants (mixture of PFDA, GMA and PETMP) and product (fluorinated epoxy).

Figure 4 shows the 1H-NMR spectra of the reactants (tmixture of PETMP, GMA, and PFDA) and the products (fluorinated epoxy).

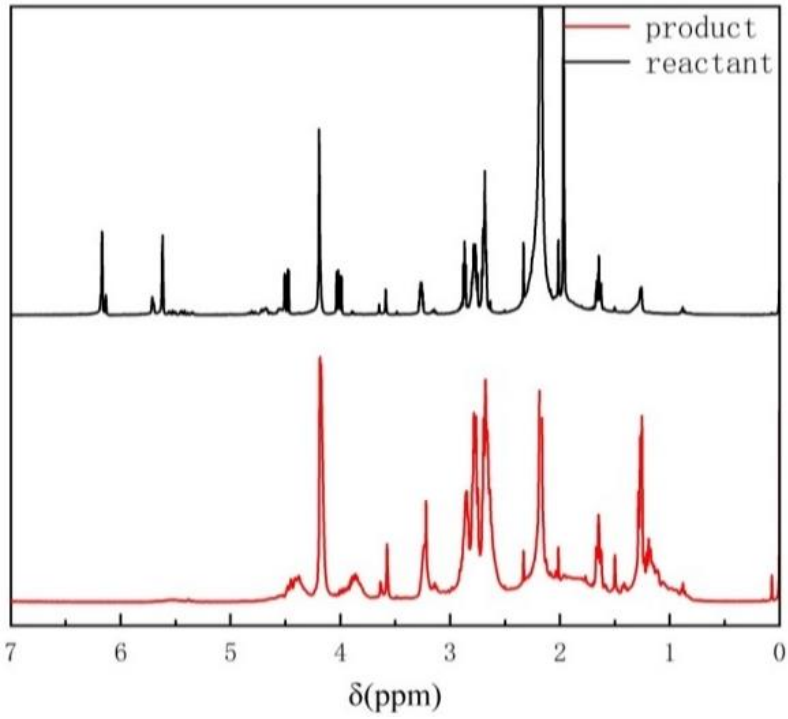

Figure 4. 1H-NMR spectra of the reactants (mixture of PFDA, GMA and PETMP) and product (fluorinated epoxy).

Vinyl terminal signals in GMA and PFDA were observed at 5.7–6.4 ppm in the 1 H-NMR spectra of the reactants. After the thiol-ene click reaction, the signal at 5.7–6.4 ppm disappeared, and the peak intensity of the methylene proton was enhanced at 2.6–2.8 ppm. In addition, the signal quantification of the methyl proton observed at 1.9 ppm adjacent to the GMA terminal double bond shifted to 1.2 ppm [47] owing to the change in chemical state of the methyl proton. The aforementioned observations prove that PETMP was successfully modified by GMA and PFDA to form the expected structure.

Although the molar ratio of GMA, PETMP and PFDA was 3:1:1, the four -SH groups on PETMP had the same probability of reacting with GMA and PFDA. Therefore, it is assumed that the case of four SH groups on PETMP reacting with GMA was C_4^0, the case of four SH groups on PETMP reacting with PFDA was C_4^4, the case of one SH group on PETMP reacting with GMA and three SH reacting with PFDA was C_4^1, the case of one SH group on PETMP reacting with PFDA and three SH reacting with GMA was C_4^3, the case of two SH group reacting with PFDA and two SH reacting with GMA was C_4^2. Thus there were $C_4^0 + C_4^1 + C_4^2 + C_4^3 + C_4^4$ cases in total. Therefore, the branched structure of fluorinated epoxy consisted of A2B2 (A is the group of PFDA in the fluorinated epoxy, and B is the group of GMA in the fluorinated epoxy), A1B3, A3B1, A0B4, and A4B0 types that yielded 37.5%, 25.0%, 25.0%, 6.25%, and 6.25%, respectively, as per the mathematical calculations. The content of A2B2, A1B3, A3B1, A0B4 and A4B0 were calculated as follows.

$$\begin{aligned} C_4^2 / \left(C_4^0 + C_4^1 + C_4^2 + C_4^3 + C_4^4\right) &= 37.5\%, \ (\text{A2B2}) \\ C_4^1 / \left(C_4^0 + C_4^1 + C_4^2 + C_4^3 + C_4^4\right) &= 25\%, \ (\text{A1B3}) \\ C_4^3 / \left(C_4^0 + C_4^1 + C_4^2 + C_4^3 + C_4^4\right) &= 25\%, \ (\text{A3B1}) \\ C_4^0 / \left(C_4^0 + C_4^1 + C_4^2 + C_4^3 + C_4^4\right) &= 6.25\%, \ (\text{A0B4}) \\ C_4^4 / \left(C_4^0 + C_4^1 + C_4^2 + C_4^3 + C_4^4\right) &= 6.25\%, \ (\text{A4B0}) \end{aligned} \quad (1)$$

As the molecule synthesized by the thiol-ene click reaction of PETMP and GMA contains both epoxy groups and long perfluoroalkyl chains, it had significant adhesion strength

with the matrix, and also made the coating itself hydrophobic (WCA was approximately 105.3 ± 0.7°).

3.2. Wetting Behavior and Mechanical Durability of the Coating

As the epoxy groups in fluorinated epoxies can react with Si–OH on silica and GC, the coating had a good bonding strength with the substrate and high mechanical durability. The composite system of micro-SiO_2 and nano-SiO_2 particles in the coating can improved the roughness of the surface, and the appropriate proportion of micro and nanoparticles can form a special re-entrant structure, which was the key for the establishment of a superhydrophobic and oleophobic coating.

The wetting behavior of the coatings were evaluated by measuring the CAs for both low- and high-surface-tension liquids, including water, glycerin, glycol, and diiodomethane. The results are shown in Table 2 and Figure 5g. When the total amount of fixed silica was 10% of the mass of fluorinated epoxy, the mass ratio of nano- and micron-silica showed a significant effect on the repellant properties for different liquids. By the addition of micron silica into the fluorinated epoxy, the liquid repellency of the coating was poor, and WCA of coating was only 123.4 ± 2.3°. With an increase of nano silica content in the silica particles, the CA of the coating for four liquids increased significantly. That is because the addition of nano particles could change the micro/nanostructure of the coating. When the amounts of nano-SiO_2 and micron-SiO_2 were equal (5 wt% nano-silica and 5 wt% micro-silica of fluorinated epoxy), the CA of the coating for four liquids reached the maximum value, and we named this coating with the best liquid repellent performance as FEP-S. Figure 5a–d shows the state of different liquids on the FEP-S coating, including water droplet (72.8 $mN{\cdot}m^{-1}$), glycerol (64.0 $mN{\cdot}m^{-1}$), ethylene glycol (47.7 $mN{\cdot}m^{-1}$) and diiodomethane (50.8 $mN{\cdot}m^{-1}$). The liquid droplets could easily roll on the sloping surface. The SAs of the different liquids are listed in Table 3. With further increase in nano-SiO_2, agglomeration of nano-SiO_2 appeared, indicating that the nano-SiO_2 could not be uniformly dispersed on the surface of micron-SiO_2 to form a re-entrant structure, and the CA for four liquids decreased at the same time. In the presence of only nano-SiO_2, the liquid repellent property of the coating surface was similar to that of only micron-SiO_2, and the superhydrophobic effect was not achieved. In Section 3.3, we will further discuss the effect of the proportion of micro/nano particles on the structure and liquid repellency of the coating.

Table 2. CAs for different liquids of fluorinated epoxy coatings with different proportions of micro/nano-silica.

CAs (°)	Water	Glycerol	Glycol	Diiodomethane
micro:nano = 1:0	123.4 ± 2.3	105.8 ± 1.4	127.3 ± 1.1	113.6 ± 1.3
micro:nano = 2:1	135.3 ± 0.8	110.4 ± 1.3	128.6 ± 1.5	118.5 ± 2.1
micro:nano = 1:1	158.6 ± 1.1	140.7 ± 0.9	152.4 ± 0.9	153.4 ± 1.3
micro:nano = 1:2	125.2 ± 1.5	120.5 ± 1.5	132.7 ± 1.4	120.8 ± 1.8
micro:nano = 0:1	120.7 ± 2.7	114.4 ± 1.8	118.5 ± 1.7	108.5 ± 2.4

Table 3. SAs for different liquids of FEP-S coatings (proportions of micro/nano-silica is 1:1).

SAs (°)	Water	Glycerol	Glycol	Diiodomethane
FEP-S	8.6 ± 1.1	14.6 ± 1.2	18.4 ± 1.5	17.5 ± 1.4

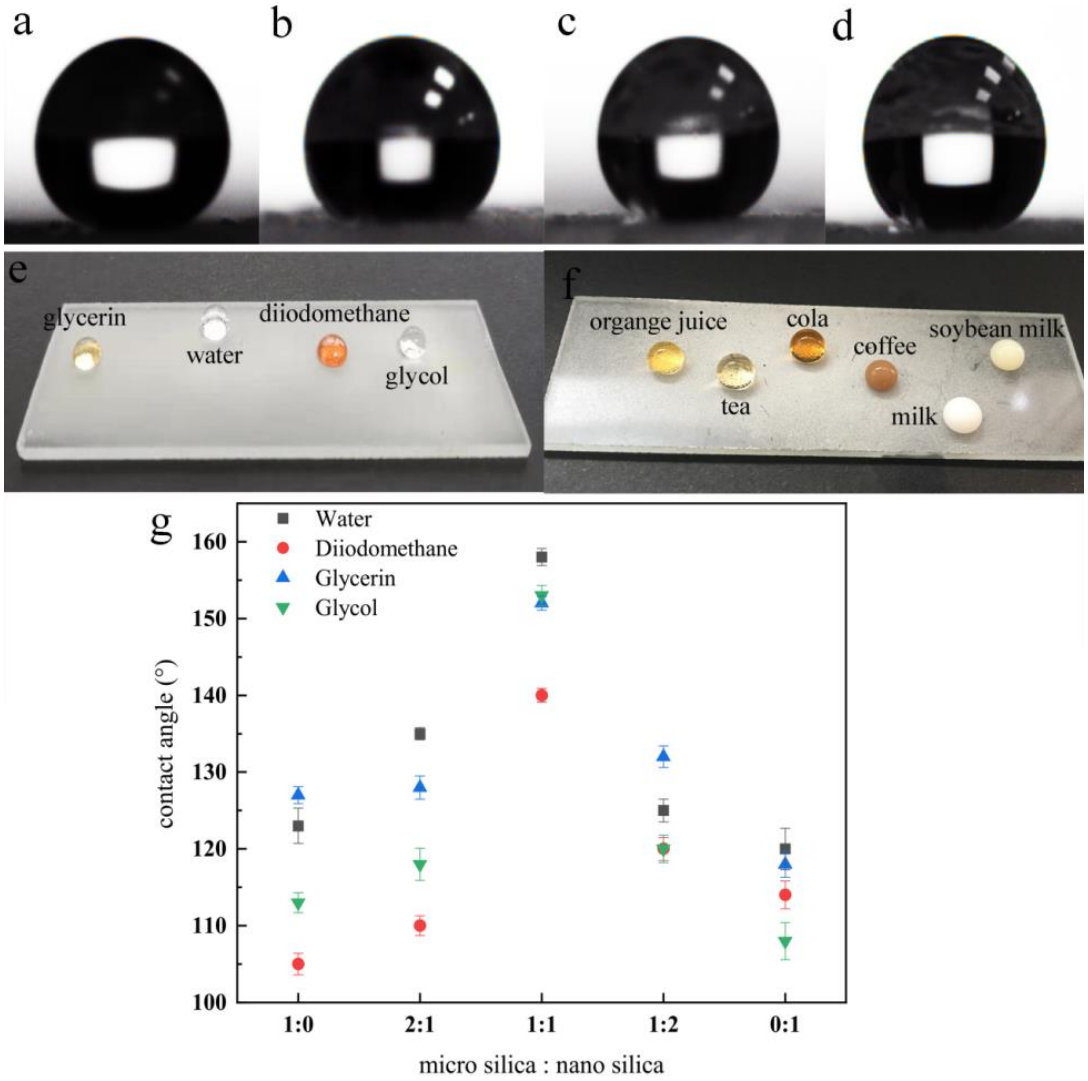

Figure 5. CAs of FEP-S slide for (**a**) water (**b**) diiodomethane (**c**) glycerol and (**d**) ethylene glycol (**e**,**f**) droplets of different liquids on FEP-S slide (**g**) CA for different liquids of coatings with different proportions of micro/nano-silica.

Durability is an important factor affecting the application of superhydrophobic materials. In particular, mechanical friction will lead to the damage of micro/nanostructures on the surface, and even slight scraping will cause function failure and loss of superhydrophobicity. Various methods are used to assess wear resistance, including sandpaper wear tests, sand/water impact, knife scraping, and tape stripping tests. In this study, the most extensive sandpaper wear test and a cross cut test were employed to evaluate the wear resistance and adhesion of the coating, respectively.

To investigate the effect of the proportion of micron- and nano-silicon on the adhesion of the coating, five coatings with different proportions of micron- and nano-silica (the mass ratio of silica particles was constant, and it was 10 wt% of fluorinated epoxy) was tested using a cross cut test. It was observed that the adhesion of all the five coatings was at level 0, indicating no falling-off of any grid or intersection, and the surface was perfect after cross cutting. In addition, when the silica particles was 10 wt% of the proportion of the fluorinated epoxy, silica particles could evenly disperse and cross-link with the fluorinated epoxy. When the fluorinated epoxy was completely cured in the presence of GC, the silica and fluorinated epoxy composite system exhibited a significant adhesion strength with the substrate.

The mass ratio of silica particles and fluorinated epoxy has an influence on the adhesion strength. In this study, the adhesive strength of the coating with different amounts of

silica particles (including micro and nano silicon, and the ratio of nano-silica and micron silica is 1:1) was explored. Consequently, when silica particles reached 10% of the mass of fluorinated epoxy (FEP-S coating), the adhesion strength of the coating was at grade 0 (the optimal level). When silica particles were 20% of the fluorinated epoxy, the adhesion strength of the coating was insignificant. Meanwhile, the bumps of silica on the coating surface could be easily taped off. The damaged area was 5% or less, and the adhesion was at level 1. When the amount of silica particles reached 30% of the mass of the fluorinated epoxy, the silica particles aggregated. The bumps of silica on the coating surface were evident, and the particles on the intersection of the grid edge were observed, which could be easily removed. The total damaged area was less than 15%, and its adhesion grade was 2.

Here, an FEP-S coating with the best liquid repellent performance was selected to test the wear resistance. The operational steps are shown in Figure 6a. A 600 mesh sandpaper was placed on a horizontal surface, and the coating was placed on the sandpaper to make the better contact of coating with the sandpaper. A 100 g weight was placed on the back of the coating, and the coating was slide along the ruler at 1 cm/s on the sandpaper surface, 10 cm toward the right and 10 cm toward the left for a cycle test. The CA of four liquids was measured after every 10 cycles, as shown in Figure 6c. The liquid repellent property of the coating to the four liquids decreased with an increase in the friction. This is because the micro/nanostructures on the surface of the coating were slightly destroyed after the sandpaper test, resulting in the loss of the rough structure. After 50 wear cycles, the coating still exhibited superhydrophobic ability, indicating that the WCA was still greater than 150.0°.

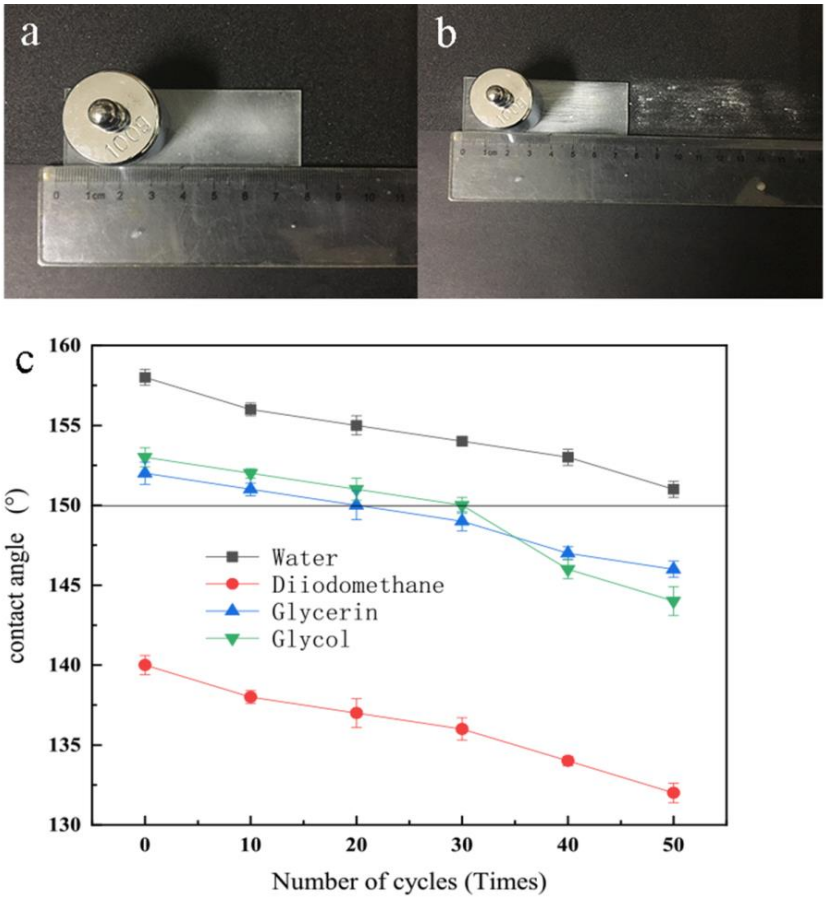

Figure 6. Image of the FEP-S coating (**a**) before and (**b**) after sandpaper abrasion at 10 m, (**c**) CA of four liquids changes of the FEP-S with sandpaper abrasion cycles.

As the thickness had a certain influence on the mechanical stability of the coating, especially on the abrasion resistance, the thickness of the FEP-S coating before and after sandpaper abrasion at 10 m was measured by SEM.

Figure 7a shows a cross-sectional SEM image of the FEP-S coating, and the thickness of FEP-S was approximately 110.7 μm, which was higher than the superhydrophobic or superoleophobic coatings (50–100 μm) prepared by the spray method in the literature [49,50]. From the SEM images (Figure 7b) after abrasion at a distance of 10 m, the thickness of FEP-S coating was down to 35.6 μm, and the substrate surface was fully covered by the superhydrophobic coating. The large thickness of the FEP-S coating was one of the reasons for its good mechanical properties.

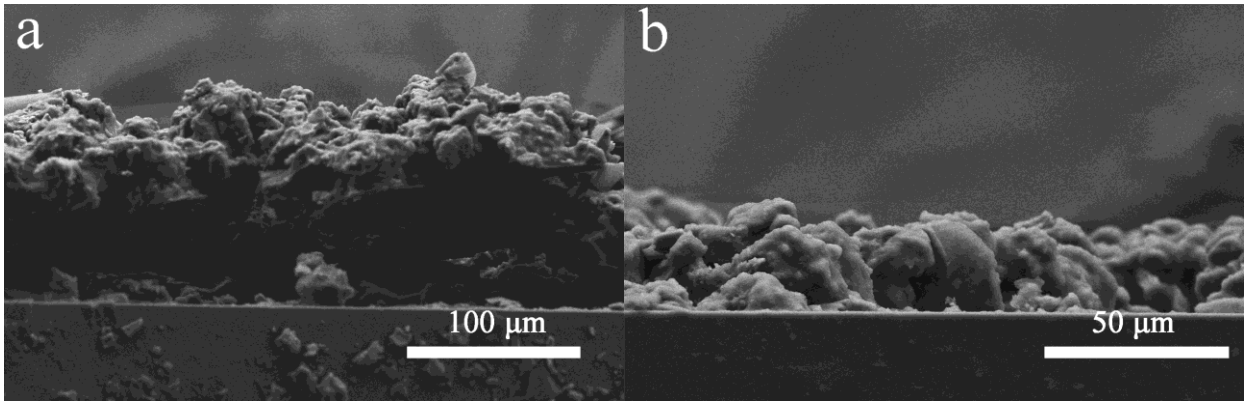

Figure 7. Cross-sectional SEM image of FEP-S coating (**a**) before and (**b**) after sandpaper abrasion at 10 m.

3.3. Surface Chemical Composition and Morphology

Figure 8(a_1–e_1) are the SEM images of S1–S5 coatings at 500× magnification, Figure 8(a_2–e_2) show the SEM images of S1–S5 coatings at 20,000× magnification, and Figure 8(f_1,f_2) show the SEM images of S5 at 35,000× and 60,000× magnifications. It can be observed that the particles on the five coatings were uniformly coated by fluorinated epoxy resin, and different micro/nanostructures are seen. Figure 8a shows that the surface of S1 coating (pure micron silica) was relatively flat, and nanoscale-bulges are not evident. From Figure 5g, the WCA of S1 coating was only 123.4°. Thus, the structure of S1 coating did not lead to the appearance of superhydrophobicity. In Figure 8b (pure nano-silica), the scale of the silica bump on the coating was approximately 2–30 μm, and the micronipples in the figure are marked by red circles. It can be seen that the degree of roughness of the coating was greater than that of pure micron silica. However, no nanoscale bulges were observed on the surface, because the agglomeration of nanoparticles coated with fluorinated epoxy forms a micron-scale structure, which had fewer nanoscale convex structures. As shown in Figure 8c (the ratio of nanoparticles to micron particles was 2:1), the surface morphology was similar to that in Figure 8b, but the size of micronipples was reduced and the distribution was more uniform, because the introduction of micron silica helped the dispersion of nano-silica. However, the introduction of a small amount of micron silica still failed to solve the problem of agglomeration of nano-silica particles, which is still unable to form nanoscale protrusion structures. When the ratio of nanoparticles to micron particles was 1:2, nano-silica particles were more evenly distributed on the micronipples and formed a nanoparticle bump (marked with a red circle in Figure 8d) at the same time. The results show that when the amount of micron silica was larger than that of nano-silica, the micro/nanostructure was formed on the surface, but the air gap structure that was formed could not retain the drop in the Cassie–Baxter state. Therefore, the liquid repellent performance of the coating at this ratio of micron/nano-silica was not the best. Figure 8e shows the SEM image of the coating surface (the ratio of nanoparticles to micron particles was 1:1); it is clear that the coating had a relatively uniform nanoscale roughness, and micron particles and aggregates also existed. In this case, the coating exhibited the best

superhydrophobic and oleophobic properties. Figure 8f shows an enlarged image of S5 coating. Micronipples from nanoscale particle aggregates (diameters in the range of 0.5–1 μm) and nanoparticle bumps (diameters of ~50 nm) appeared, and we could see a large air gap between the micronipples. This structure was the same as the re-entrant structure, which allowed air to exist beneath the liquid droplet and causes the low-surface-tension droplet to remain Cassie–Baxter state on the surface. This forms the basis for repellency to water and low-surface-tension liquids, such as ethylene glycol.

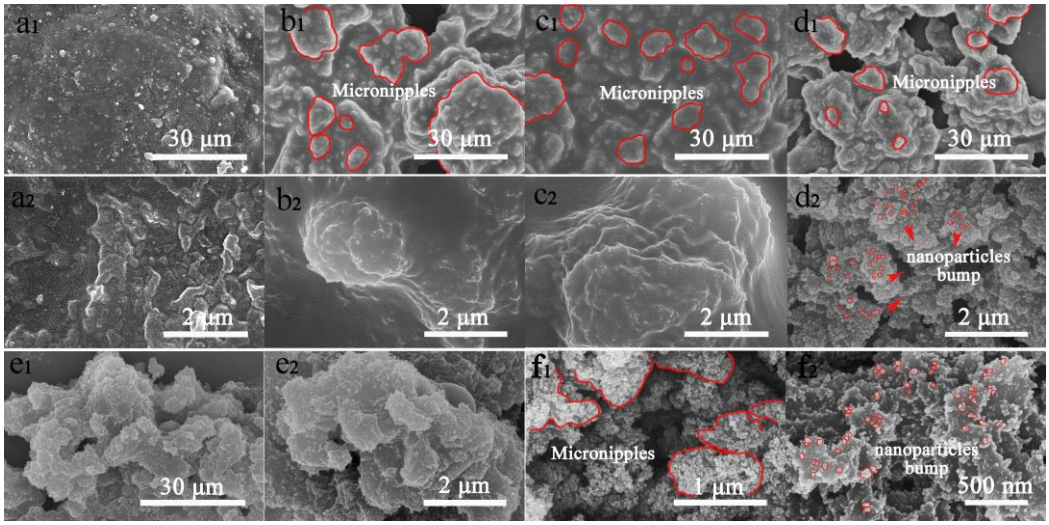

Figure 8. SEM image of fluorinated epoxy coating with different proportions of micro- and nano-silica (The mass ratio of nano-silica and micro-silica particles: (**a1**,**a2**) 0:1, (**b1**,**b2**) 1:0, (**c1**,**c2**) 2:1, (**d1**,**d2**) 1:2, (**e1**,**e2**) 1:1 and (**f1**,**f2**) 1:1 energy-dispersive X-ray spectroscopy (EDS) and X-ray photoelectron spectroscopy (XPS) were used to analyze the chemical composition of the FEP-S coating. C, O, F, and Si were detected in the EDS mapping shown in Figure 9; all elements were uniformly distributed.

Figure 9g shows the XPS spectrum in which some peaks corresponding to C1s (291.3 eV), O1s (532.2 eV), F1s (688.3 eV), and Si2p (101.8 eV) are presented. Figure 9e presents the high-resolution spectrum of C1s; the CF_2 (291.3 eV), CF_2-CH_2 (288.4 eV), C=O (288.9 eV), C-O/C-N and C-S (286.2 eV), and C-C/C-H (284.7 eV) peaks were detected. The absence of the peak of CF_3 in the high-resolution spectrum of C1s may be owing to the fact that CF_2 groups were mainly in the long perfluoroalkyl chains. Figure 9f shows the high-resolution spectrum of F1s, in which three fitting peaks could be assigned to CF_3 (689.3 eV), CF_2 (688.1 eV), and CF_2-CH_2 (686.9 eV), indicating the presence of a low surface energy -CF_3 group on the coating surface.

It can be seen from XPS that the amount of element F on the surface of the aluminum foil was only 11.9%, and it primarily existed in the form of CF_2 and CF_3 on the surface of the sample (located at 291.3 eV). This is because the long perfluoroalkyl chains on the PFDA molecule were grafted to the fluorinated epoxy molecule. The nano- and micron-silica were not treated with fluorosilane, so the fluorine content on the surface was low, which indicates that the properties of superhydrophobic and oleophobic of the coating was provided by the micro/nano rough structure on the surface and the low surface energy of fluorinated epoxy. Meanwhile, the Si content on the surface of the coating was only 2.64%, which means that the fluorinated epoxy covered most of the surface of the coating, so the coating exhibited good adhesion strength and wear resistance.

3.4. Chemical Stability

Corrosion resistance is an important property of superhydrophobic coating, which determines whether the coating can be applied in acidic or alkaline environment. Therefore, we characterized the chemical stability of the coating by two methods. Water droplets with pH values of 1–14 were placed on the surface of the FEP-S coating to test the chemical

stability of the coating (as shown in Figure 10). Results show that droplets rolled on the coating without sticking. This indicates that the coating had strong repellent ability toward distilled water as well as a corrosive solution.

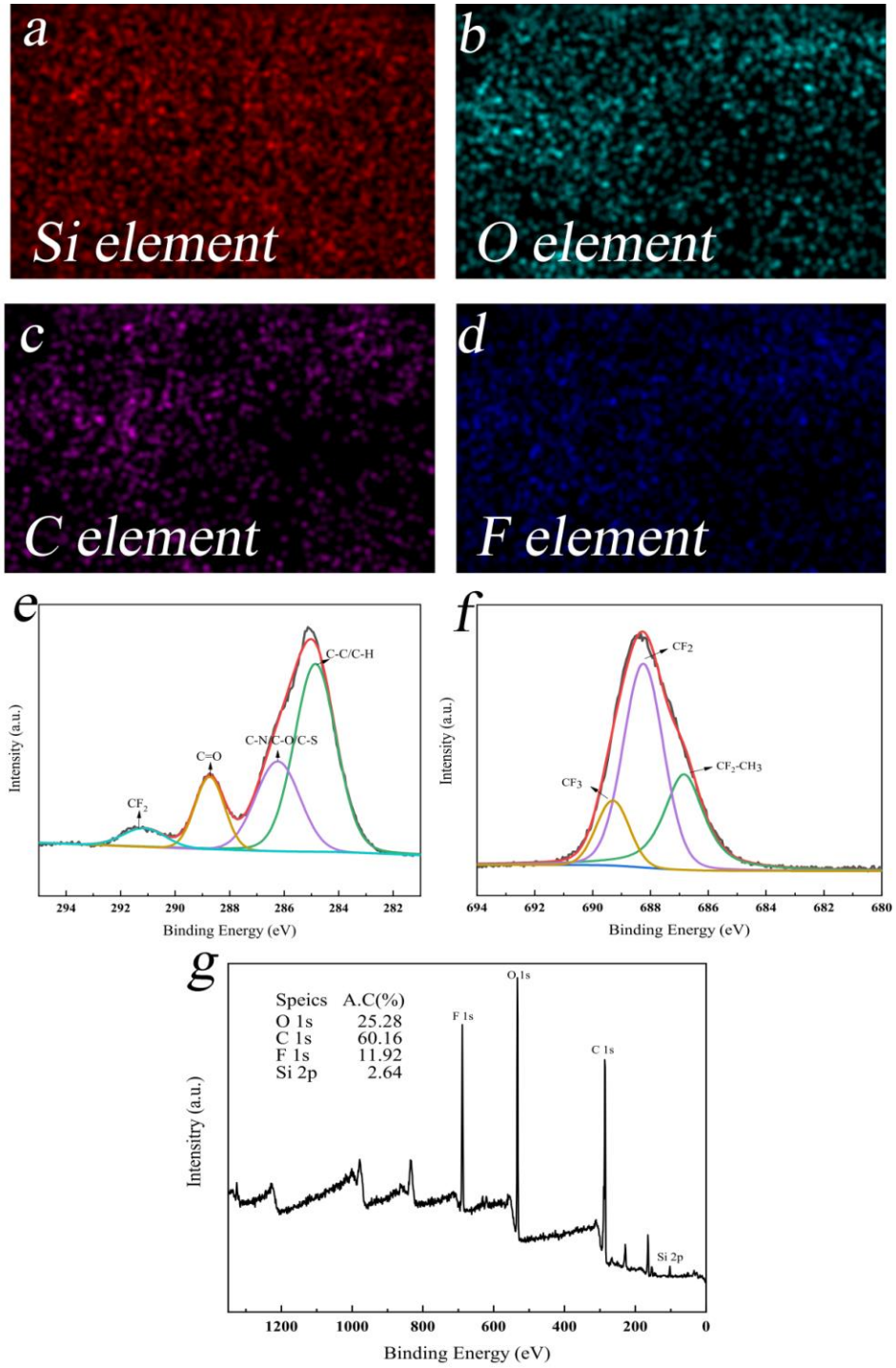

Figure 9. (**a**–**d**) EDS mapping, (**e**) high-resolution C1s spectra, (**f**) high-resolution F1s spectra and (**g**) XPS survey spectra of FEP-S coating.

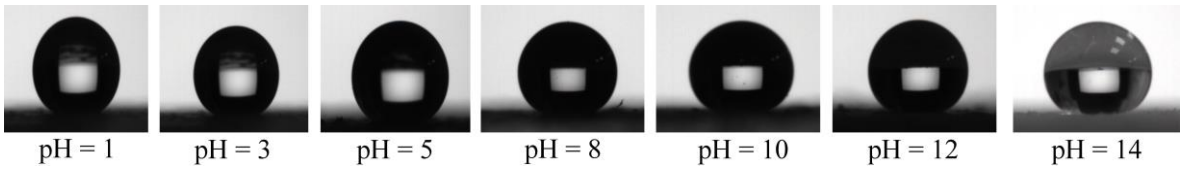

Figure 10. Shape of different pH solution droplets on FEP-S coating.

For further evaluation, chemical corrosion resistance of FEP-S in strong acidic and alkaline environments, the coating was placed in 1 mol/L hydrochloric acid and sodium hydroxide for 1 h, and then taken out, washed with distilled water for 3 min, and dried in an oven at 80 °C for 10 min. The CAs of FEP-S for water, glycerol, diiodimethane, and ethylene glycol are listed in Table 4.

Table 4. CA of FEP-S for different liquids after immersion in HCl and NaOH solution for 1 h.

CAs (°)	Water	Glycerol	Diiodomethane	Glycol
1M HCl	158.4 ± 0.8	152.5 ± 0.7	135.3 ± 1.1	147.5 ± 0.9
1M NaOH	157.6 ± 0.7	153.7 ± 0.6	136.4 ± 0.9	148.6 ± 1.2

As can be seen from Table 4, the FEP-S coating was still superhydrophobic after immersion in strong acid and alkali for 1 h. The WCA was approximately 158.0°, and the CA for glycerol is more than 150.0°. Meanwhile, the CAs for diiodide and ethylene glycol was still very high. The as-prepared FEP-S coating had excellent chemical stability and good acid and alkali resistance. This can be attributed to the long perfluoroalkyl chains on the FEP-S coating, silica, and the epoxy itself.

3.5. Self-Cleaning Properties

Lotus leaves have a natural superhydrophobic surface and good self-cleaning ability. The rolling of water droplets on the lotus leaves automatically carried away dust and kept the surface clean. An oil-free superhydrophobic surface can prevent the surface damage caused by oil to maintain self-cleaning ability for a long time. Figure 11 shows the repellent properties of the coating for common liquids, including orange juice, soy milk, black tea, coffee, cola, and milk. The FEP-S coating was immersed in these solutions for 5 min, and no liquid drops were found on the glass sheet, indicating that the coating was difficult to be polluted by common liquids in daily life.

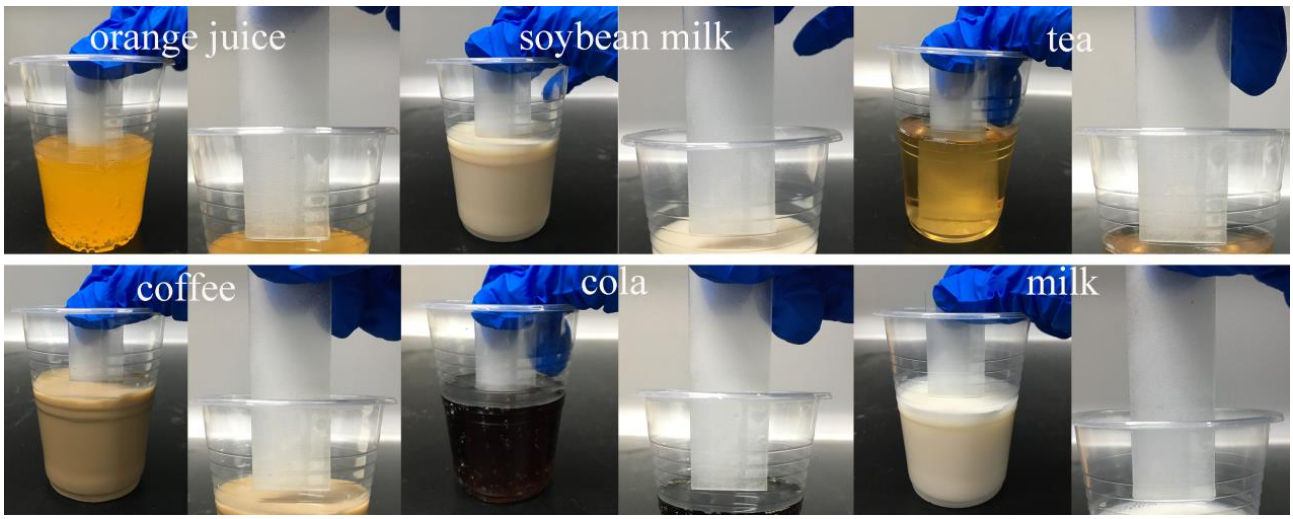

Figure 11. Repellent properties of the FEP-S coatings for common liquids.

We used carbon black powder insoluble in water (which is harder to be cleaned than general dusts) and $CuSO_4$ powder soluble in water as pollutant to test the self-cleaning performance of the FEP-S coating. First, $CuSO_4$ powder and carbon black powder were evenly distributed over the surface as shown in Figure 12. Subsequently, water was dropped on the surface. It can be observed that pollutants easily rolled away from the surface along with the rolling of water droplets. The surface polluted by dust was cleaned in a short time, presenting the same clean surface state as before. Thus, in practical applications, the FEP-S coating could efficiently protect the substrate from dusts and other pollutants. These properties made the FEP-S coating able to be applied to more practical applications, such as kitchenware, exterior wall, oil pipeline, clothing etc.

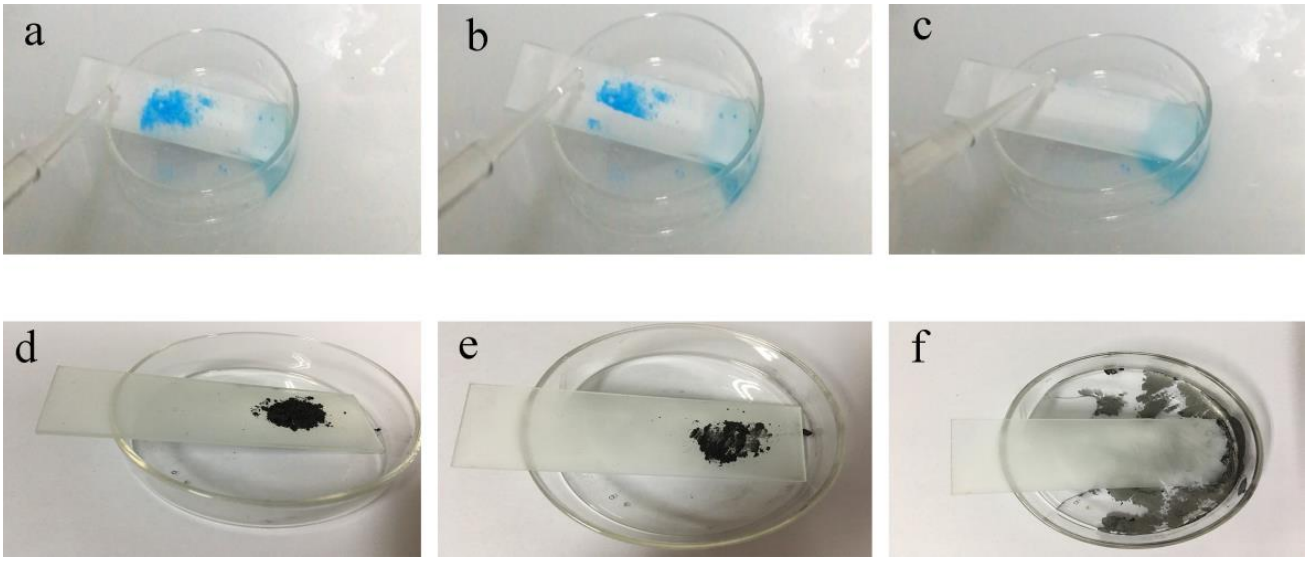

Figure 12. Self-cleaning behavior of FEP-S coating using (**a**–**c**) $CuSO_4$ powder and (**d**–**f**) carbon black powder as contaminants.

3.6. Anti-Icing Performance

Ice often causes problems in transportation, such as power transmission and wind power generation. The reasonable construction of a superhydrophobic surface is promising for the application of anti-icing. In order to test the anti-icing performance of the FEP-S coating, a drop of water (~0.05 mL) was dropped on the original glass sheet and the glass sheet was sprayed with FEP-S coating, and the glass sheets were placed in a refrigerator at −18 °C. The glass sheets were taken out every 30 s to observe the state of water droplets on the surface.

On the bare glass slide, the water drop began to freeze at ~15 s and was completely frozen at ~30 s (Figure 13). On the coated glass slide, the water drop began to freeze at 5 min and was completely frozen at 10 min. This means that the FEP-S coating could delay icing by ca. 10 min in extremely freezing weather. This may be due to the small solid–liquid contact area of the water droplets on the FEP-S coating. At the same time, the contact anchorage point was very small, so the ice adhesion strength was low, and the ice drop could be lightly removed from the coating by a slight jerk of a pipette.

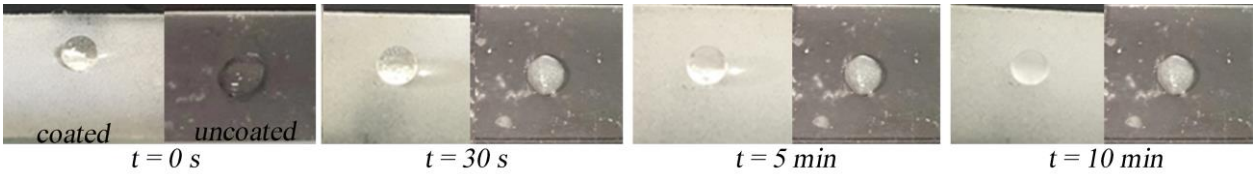

Figure 13. Anti-icing properties of FEP-S coating.

In order to further observe the dynamic icing behavior of the FEP-S coating, we placed the FEP-S coating in the freezer at −18 °C for 24 h, and then dropped 0 °C water drops from the ice water mixture to observe the state of the water droplets. As shown in Video S1, the FEP-S coating placed at −18 °C for 24 h still exhibited good superhydrophobicity. Once the water drops fell on the surface of the coating, it rebound quickly, which means that the water drops bounced off the coating and rolled away before the temperature of the water drops to the freezing point.

The results show that the FEP-S coating had good static and dynamic anti-icing performance in extremely freezing weather. Even in extreme cold conditions, the coating still had superhydrophobic and anti-icing properties, which made the FEP-S coating still have certain self-cleaning and anti-fouling ability.

4. Conclusions

To summarize, we have successfully synthesized a fluorinated epoxy containing an epoxy group and long perfluoroalkyl chains by a thiol-ene click reaction. We have constructed a re-entrant-like structure by adding different proportions of unmodified nano- and micro-silica into the fluorinated epoxy, and obtain the superhydrophobic and oleophobic surface with excellent comprehensive properties. The as-prepared FEP-S surface exhibits high CA and low SA for water, with WCA higher than 158.6° ± 1.1° and SA lower than 10°, and the CAs for glycerol, ethylene glycol, and diiodomethane reached 152.4° ± 0.9°, 153.4° ± 1.3°, and 140.7° ± 0.9°, respectively.

In addition, the coating exhibited good durability. After sandpaper abrasion for 10 m, FEP-S surface still had good amphiphobicity. The fabricated FEP-S surface exhibits excellent performance in self-cleaning, corrosion resistance, and anti-icing. The coating also showed a remarkable durability towards strong acid and alkali.

Supplementary Materials: The following are available online at https://www.mdpi.com/article/10.3390/coatings11060663/s1, Video S1: Anti-Icing Performance of FEP-S Superhydrophobic Coatings.

Author Contributions: Conceptualization, R.Y.; investigation, X.H.; project administration, R.Y.; software, X.H.; supervision, R.Y.; writing—original draft, X.H. All authors have read and agreed to the published version of the manuscript.

Funding: This research received no external funding.

Institutional Review Board Statement: Not applicable.

Informed Consent Statement: Not applicable.

Data Availability Statement: Data sharing not applicable. No new data were created or analyzed in this study. Data sharing is not applicable to this article.

Conflicts of Interest: The authors declare no conflict of interest.

References

1. Zhang, H.; Ma, Y.; Tan, J.J.; Fan, X.L.; Liu, Y.B.; Gu, J.W.; Zhang, B.L.; Zhang, H.P.; Zhang, Q.Y. Robust, self-healing, superhydrophobic coatings highlighted by a novel branched thiol-ene fluorinated siloxane nanocomposites. *Compos. Sci. Technol.* **2016**, *137*, 78–86. [CrossRef]
2. Chen, J.H.; Liu, Z.H.; Wen, X.F.; Xu, S.P.; Wang, F.; Pi, P.H. Two-Step Approach for Fabrication of Durable Superamphiphobic Fabrics for Self-Cleaning, Antifouling, and On-Demand Oil/Water Separation. *Ind. Eng. Chem. Res.* **2019**, *58*, 5490–5500. [CrossRef]

3. Wang, H.H.; Lu, H.T.; Zhang, X. Super-robust superamphiphobic surface with anti-icing property. *RSC Adv.* **2019**, *9*, 27702–27709. [CrossRef]
4. Li, Y.; Hu, T.; Li, B.; Wei, J.; Zhang, J. Totally Waterborne and Highly Durable Superamphiphobic Coatings for Anti-Icing and Anticorrosion. *Adv. Mater. Interfaces* **2019**, *6*. [CrossRef]
5. Su, F.; Yao, K. Facile fabrication of superhydrophobic surface with excellent mechanical abrasion and corrosion resistance on copper substrate by a novel method. *ACS Appl. Mater. Interfaces* **2014**, *6*, 8762–8770. [CrossRef]
6. Zhang, B.; Xu, W.; Xia, D.; Huang, Y.; Zhao, X.; Zhang, J. Spray coated superamphiphobic surface with hot water repellency and durable corrosion resistance. *Colloid Surf. A* **2020**, *596*. [CrossRef]
7. Wang, H.; Zhou, H.; Niu, H.; Zhang, J.; Du, Y.; Lin, T. Dual-Layer Superamphiphobic/Superhydrophobic-Oleophilic Nanofibrous Membranes with Unidirectional Oil-Transport Ability and Strengthened Oil-Water Separation Performance. *Adv. Mater. Interfaces* **2015**, *2*. [CrossRef]
8. Wang, H.; Zhang, Z.; Wang, Z.; Liang, Y.; Cui, Z.; Zhao, J.; Li, X.; Ren, L. Multistimuli-Responsive Microstructured Superamphiphobic Surfaces with Large-Range, Reversible Switchable Wettability for Oil. *ACS Appl. Mater. Inter.* **2019**, *11*, 28478–28486. [CrossRef]
9. Tuteja, A.; Choi, W.; Ma, M.; Mabry, J.M.; Mazzella, S.A.; Rutledge, G.C.; McKinley, G.H.; Cohen, R.E. Designing superoleophobic surfaces. *Science* **2007**, *318*, 1618–1622. [CrossRef]
10. Telecka, A.; Li, T.; Ndoni, S.; Taboryski, R. Nanotextured Si surfaces derived from block-copolymer self-assembly with superhydrophobic, superhydrophilic, or superamphiphobic properties. *RSC Adv.* **2018**, *8*, 4204–4213. [CrossRef]
11. Tuominen, M.; Teisala, H.; Haapanen, J.; Makela, J.M.; Honkanen, M.; Vippola, M.; Bardage, S.; Walinder, M.E.P.; Swerin, A. Superamphiphobic overhang structured coating on a biobased material. *Appl. Surf. Sci.* **2016**, *389*, 135–143. [CrossRef]
12. Huang, L.; Yao, Y.; Peng, Z.; Zhang, B.; Chen, S. How to Achieve a Monostable Cassie State on a Micropillar-Arrayed Superhydrophobic Surface. *J. Phys. Chem. B.* **2021**, *125*, 883–894. [CrossRef]
13. Zhu, C.; Gao, Y.; Huang, Y.; Li, H.; Meng, S.; Francisco, J.S.; Zeng, X.C. Controlling states of water droplets on nanostructured surfaces by design. *Nanoscale* **2017**, *9*, 18240–18245. [CrossRef] [PubMed]
14. Chen, L.; Guo, Z.; Liu, W. Biomimetic Multi-Functional Superamphiphobic FOTS-TiO_2 Particles beyond Lotus Leaf. *ACS Appl. Mater. Inter.* **2016**, *8*, 27188–27198. [CrossRef]
15. Yao, W.; Li, L.; Li, O.L.; Cho, Y.-W.; Jeong, M.-Y.; Cho, Y.-R. Robust, self-cleaning, amphiphobic coating with flower-like nanostructure on micro-patterned polymer substrate. *Chem. Eng. J.* **2018**, *352*, 173–181. [CrossRef]
16. Li, H.; Yu, S.; Han, X. Fabrication of CuO hierarchical flower-like structures with biomimetic superamphiphobic, self-cleaning and corrosion resistance properties. *Chem. Eng. J.* **2016**, *283*, 1443–1454. [CrossRef]
17. Velayi, E.; Norouzbeigi, R. Single-step prepared hybrid ZnO/CuO nanopowders for water repellent and corrosion resistant coatings. *Ceram. Int.* **2019**, *45*, 16864–16872. [CrossRef]
18. Ge, D.; Yang, L.; Zhang, Y.; Rahmawan, Y.; Yang, S. Transparent and Superamphiphobic Surfaces from One-step Spray Coating of Stringed Silica Nanoparticle/Sol Solutions. *Part. Part. Syst. Char.* **2014**, *31*, 763–770. [CrossRef]
19. Zhi, S.; Wang, G.; Zeng, Z.; Zhu, L.; Liu, Z.; Zhang, D.; Xu, K.; Xue, Q. 3D mossy structures of zinc filaments: A facile strategy for superamphiphobic surface design. *J. Colloid Interf. Sci.* **2018**, *526*, 106–113. [CrossRef]
20. Hyuneui, L. Beyond a nature-inspired lotus surface: Simple fabrication approach part I. Superhydrophobic and transparent biomimetic glass part II. Superamphiphobic web of nanofibers. In *Advances in Biomimetics*; InTech Open: London, UK, 2011; pp. 145–158.
21. Deng, X.; Mammen, L.; Butt, H.J.; Vollmer, D. Candle soot as a template for a transparent robust superamphiphobic coating. *Science* **2012**, *335*, 67–70. [CrossRef]
22. Liu, Z.J.; Wang, H.Y.; Wang, W.Q.; Zhang, X.G.; Yuan, R.X.; Zhu, Y.J. Superhydrophobic poly(vinylidene fluoride) membranes with controllable structure and tunable wettability prepared by one-step electrospinning. *Polymer* **2016**, *82*, 105–113. [CrossRef]
23. Ganesh, V.A.; Dinachali, S.S.; Nair, A.S.; Seeram, R. Robust Superamphiphobic Film from Electrospun TiO_2 Nanostructures. *ACS Appl. Mater. Inter.* **2013**, *5*, 1527–1532. [CrossRef]
24. Li, T.; Paliy, M.; Wang, X.; Kobe, B.; Lau, W.-M.; Yang, J. Facile One-Step Photolithographic Method for Engineering Hierarchically Nano/Microstructured Transparent Superamphiphobic Surfaces. *ACS Appl. Mater. Inter.* **2015**, *7*, 10988–10992. [CrossRef]
25. Dong, S.; Zhang, X.; Li, Q.; Liu, C.; Ye, T.; Liu, J.; Xu, H.; Zhang, X.; Liu, J.; Jiang, C.; et al. Springtail-Inspired Superamphiphobic Ordered Nanohoodoo Arrays with Quasi-Doubly Reentrant Structures. *Small* **2020**, *16*. [CrossRef]
26. Stefelová, J.; Slovák, V.; Siqueira, G.; Olsson, R.T.; Tingaut, P.; Zimmermann, T.; Sehaqui, H. Drying and Pyrolysis of Cellulose Nanofibers from Wood, Bacteria, and Algae for Char Application in Oil Absorption and Dye Adsorption. *ACS Sustain. Chem. Eng.* **2017**, *5*, 2679–2692. [CrossRef]
27. Yin, K.; Dong, X.; Zhang, F.; Wang, C.; Duan, J.A. Superamphiphobic miniature boat fabricated by laser micromachining. *Appl. Phys. Lett.* **2017**, *110*. [CrossRef]
28. Wan, Y.L.; Chuan, W.X.; Liu, Z.G.; Yu, H.D.; Li, J. Preparation of superamphiphobic aluminium alloy surface based on laser-EDM method. *Micro Nano Lett.* **2018**, *13*, 281–283. [CrossRef]
29. Yin, K.; Du, H.F.; Luo, Z.; Dong, X.R.; Duan, J.A. Multifunctional micro/nano-patterned PTFE near-superamphiphobic surfaces achieved by a femtosecond laser. *Surf. Coat. Technol.* **2018**, *345*, 53–60. [CrossRef]

30. Sun, Y.W.; Wang, L.L.; Gao, Y.Z.; Guo, D.M. Preparation of stable superamphiphobic surfaces on Ti-6Al-4V substrates by one-step anodization. *Appl. Surf. Sci.* **2015**, *324*, 825–830. [CrossRef]
31. Barthwal, S.; Kim, Y.S.; Lim, S.-H. Fabrication of amphiphobic surface by using titanium anodization for large-area three-dimensional substrates. *J. Colloid Interf. Sci.* **2013**, *400*, 123–129. [CrossRef]
32. Zhang, J.; Yu, B.; Wei, Q.; Li, B.; Li, L.; Yang, Y. Highly transparent superamphiphobic surfaces by elaborate microstructure regulation. *J. Colloid Interf. Sci.* **2019**, *554*, 250–259. [CrossRef]
33. Ellinas, K.; Pujari, S.P.; Dragatogiannis, D.A.; Charitidis, C.A.; Tserepi, A.; Zuilhof, H.; Gogolides, E. Plasma Micro-Nanotextured, Scratch, Water and Hexadecane Resistant, Superhydrophobic, and Superamphiphobic Polymeric Surfaces with Perfluorinated Monolayers. *ACS Appl. Mater. Inter.* **2014**, *6*, 6510–6524. [CrossRef]
34. Cai, J.; Wang, T.; Hao, W.; Ling, H.; Hang, T.; Chung, Y.-W.; Li, M. Fabrication of superamphiphobic Cu surfaces using hierarchical surface morphology and fluorocarbon attachment facilitated by plasma activation. *Appl. Surf. Sci.* **2019**, *464*, 140–145. [CrossRef]
35. Ellinas, K.; Tserepi, A.; Gogolides, E. Superhydrophobic Fabrics with Mechanical Durability Prepared by a Two-Step Plasma Processing Method. *Coatings* **2018**, *8*, 351. [CrossRef]
36. Wang, H.; Liu, Z.; Wang, E.; Zhang, X.; Yuan, R.; Wu, S.; Zhu, Y. Facile preparation of superamphiphobic epoxy resin/modified poly(vinylidene fluoride)/fluorinated ethylene propylene composite coating with corrosion/wear-resistance. *Appl. Surf. Sci.* **2015**, *357*, 229–235. [CrossRef]
37. Li, X.; Li, H.; Huang, K.; Zou, H.; Yu, D.; Li, Y.; Qiu, B.; Wang, X. Durable superamphiphobic nano-silica/epoxy composite coating via coaxial electrospraying method. *Appl. Surf. Sci.* **2018**, *436*, 283–292. [CrossRef]
38. Yousefi, E.; Ghadimi, M.R.; Amirpoor, S.; Dolad, A. Preparation of new superhydrophobic and highly oleophobic polyurethane coating with enhanced mechanical durability. *Appl. Surf. Sci.* **2018**, *454*, 201–209. [CrossRef]
39. Huang, C.; Wang, F.; Wang, D.; Guo, Z. Wear-resistant and robust superamphiphobic coatings with hierarchical TiO_2/SiO_2 composite particles and inorganic adhesives. *New J. Chem.* **2020**, *44*, 1194–1203. [CrossRef]
40. Xiong, D.; Liu, G.; Duncan, E.J.S. Robust amphiphobic coatings from bi-functional silica particles on flat substrates. *Polymer* **2013**, *54*, 3008–3016. [CrossRef]
41. Su, C. A simple and cost-effective method for fabricating lotus-effect composite coatings. *J. Coat. Technol. Res.* **2012**, *9*, 135–141. [CrossRef]
42. Zhang, F.; Qian, H.; Wang, L.; Wang, Z.; Du, C.; Li, X.; Zhang, D. Superhydrophobic carbon nanotubes/epoxy nanocomposite coating by facile one-step spraying. *Surf. Coat. Technol.* **2018**, *341*, 15–23. [CrossRef]
43. Xiu, Y.H.; Liu, Y.; Balu, B.; Hess, D.W.; Wong, C. Robust Superhydrophobic Surfaces Prepared with Epoxy Resin and Silica Nanoparticles. *IEEE T. Comp. Pack. Man.* **2012**, *2*, 395–401. [CrossRef]
44. Han, X.; Peng, J.; Jiang, S.; Xiong, J.; Song, Y.; Gong, X. Robust Superamphiphobic Coatings Based on Raspberry-like Hollow SnO_2 Composites. *Langmuir* **2020**, *36*, 11044–11053. [CrossRef] [PubMed]
45. Peng, J.; Zhao, X.; Wang, W.; Gong, X. Durable Self-Cleaning Surfaces with Superhydrophobic and Highly Oleophobic Properties. *Langmuir* **2019**, *35*, 8404–8412. [CrossRef]
46. Aslanidou, D.; Karapanagiotis, I.; Panayiotou, C. Tuning the wetting properties of siloxane-nanoparticle coatings to induce superhydrophobicity and superoleophobicity for stone protection. *Mater. Des.* **2016**, *108*, 736–744. [CrossRef]
47. Zhu, K.; Zhang, J.; Zhang, H.; Tan, H.; Zhang, W.; Liu, Y.; Zhang, H.; Zhang, Q. Fabrication of durable superhydrophobic coatings based on a novel branched fluorinated epoxy. *Chem. Eng. J.* **2018**, *351*, 569–578. [CrossRef]
48. Zhang, H.; Tan, J.; Liu, Y.; Hou, C.; Ma, Y.; Gu, J.; Zhang, B.; Zhang, H.; Zhang, Q. Design and fabrication of robust, rapid self-healable, superamphiphobic coatings by a liquid-repellent "glue plus particles" approach. *Mater. Des.* **2017**, *135*, 16–25. [CrossRef]
49. Wang, K.L.; Liu, X.R.; Tan, Y.; Zhang, W.; Zhang, S.F.; Liu, J.Z.; Huang, A.M. Highly fluorinated and hierarchical HNTs/SiO_2 hybrid particles for substrate-independent superamphiphobic coatings. *Chem. Eng. J.* **2018**, *359*, 626–640. [CrossRef]
50. Li, Y.B.; Li, B.C.; Zhao, X.; Tian, N.; Zhang, J.P. Totally Waterborne, Nonfluorinated, Mechanically Robust, and Self-Healing Superhydrophobic Coatings for Actual Anti-Icing. *ACS Appl. Mater. Inter.* **2018**, *10*, 39391–39399. [CrossRef]